Analysing Faults and SFCL Response in Electric Aircraft

H Alafnan[14], X Zeng[2], X Pei[1], M Khedr[1], M Zhang[3], W Yuan[3]

[1]Department of Electronic and Electrical Engineering, University of Bath, Bath BA2 7AY, U.K.
[2]Department of Mechanical Engineering, University of Bath, Bath BA2 7AY, U.K
[3]Department of Electronic and Electrical Engineering, University of Strathclyde, Glasgow G1 1XW, U.K.
[4]Department of Electrical Engineering, University of Hail, Hail 55476, KSA.
E-mail: hfa25@bath.ac.uk

Abstract. Aircraft technology moves towards electrification in order to achieve environmentally friendly goals. However, one of the main challenges facing the electrification of aircraft technology is the weight of the electric devices necessary for operating a fully electric aircraft. The National Aeronautics and Space Administration (NASA) proposed the use of the superconductive technology in electric aircraft (EA) to overcome this challenge in addition to its other benefits. The proposed EA is called N3-X and it has an on-board DC superconducting network including a superconducting fault current limiter (SFCL). The SFCL is a self-mechanism device that very effectively limits the current within a few milliseconds, thus improving the stability of the system. As the grounding of this network is different from traditional networks, analysing the behaviour of different fault types and how to manage them becomes critical. In this paper, one set of the EA's systems (one generator, AC/DC rectifier and four motors with their DC/AC variable frequency drives) has been modelled in MATLAB/Simulink environment to carry out the fault analysis and to demonstrate the effect of the SFCL on this network under different types of faults.

1. Introduction

As concerns regarding global warming and air pollution grows around the world, several organisations and companies started acting towards a healthier and cleaner environment. The National Aeronautics and Space Administration (NASA) and the Advisory Council for Aviation Research and Innovation in Europe (ACARE) have set goals to reduce carbon dioxide (CO_2) and nitrogen oxide (NO_x) emissions, as well as the external noise levels of commercial aircraft. These environmental goals are shown in Table 1 and are relative to the levels from the 2000 [1–3].

TABLE I
NASA AND ACARE ENVIRONMENTAL GOALS

Category	ACARE 2020	ACARE 2050	NASA N+2 ~2020	NASA N+3 ~2030
CO_2 reduction	50%	75%	-	-
NO_x reduction	80%	90%	75%	80%
Noise reduction	50%	65%	-42 dB	-71dB
Fuel burn	50%	-	50%	60%

Because the current hydraulic, pneumatic, and mechanical actuators in conventional aircraft are relatively inefficient (~40%) [4], moving towards Electrical Aircraft (EA) is a promising solution to achieve environmentally friendly goals such as the ones in Table 1 [5]. One of the obvious solutions is the use of batteries as the energy source. Currently, few electric aircraft operate battery-only systems, including the E-Fan. E-Fan was a two-seat fully electric aircraft powered by a battery-only system produced by Airbus for pilot training and two-seat touring in 2014 [6]. However, while it is possible to fly ultra-light and small-size aircraft with battery-only systems, it is not possible to fly commercial aircraft with over 100 passengers with battery-only systems due of the low energy density (kWh/kg) of batteries 320 Wh/kg [7]. Airbus, along with its partners Rolls-Royce and Siemens, have started a new hybrid-electric propulsion project for commercial aircraft, named the E-Fan X. The testbed of the E-Fan X is based on replacing one of its four turbofans with a 2 MW electric motor, and the E-Fan X is anticipated to fly in 2020 [8]. Another such project was the UK government-funded Distributed Electrical Aerospace Propulsion (DEAP) project where Airbus, Rolls Royce, and Canfield University investigated the feasibility of distributed propulsion systems in aircraft by using two gas-driven high temperature superconducting (HTS) turbo-generators and eight HTS motor-driven fans to produce the require thrust [9].

NASA introduced the concept of Turboelectric Distributed Propulsion (TeDP) systems in 2005. The main idea of TeDP is relocating the gas turbine engines away from the propulsors, resulting in the EA's power architecture to look like a small microgrid with a number of gas turbine engines and motors connected to fans or propellers, allowing for the hybridization of energy sources and the implementation of superconducting fault current limiters (SFCL) to improve the system's performance [10].

The most notable EA concept is NASA's N3-X and was proposed under NASA's Research and Technology for Aerospace Propulsion (RTAPS) initiative [11]. N3-X is a DC microgrid on-board, which consists of sixteen motors, four generators, and several electrical devices including rectifiers, inverters, circuit breakers, and SFCL [10]. A SFCL is a self-mechanism device that provides very effective current limitation within a few milliseconds of a fault occurring [13–15]. When the current exceeds the critical current ($I_{critical}$), the resistivity of the superconducting coil increases quickly, reducing the system's maximum fault current.

The on-board installed electrical power systems and the overall network of the electric aircraft face several design challenges, including the grounding of this network. In order to carry out the fault analysis and to demonstrate the effect and importance of the SFCL in the EA, one set of the EA's systems, as shown in Fig. 1, has been modelled in MATLAB/Simulink environment.

2. System Description

The N3-X TeDP power system architecture, the Inner Bus Tie Concept (IBTC), proposed by NASA [10], was chosen as the platform for carrying the fault analysis of the EA and the SFCL response. In this paper, one set of the power system architecture of the N3-X has been modelled, with four motors (1.86 MW each) and one generator (14.91 MW) as shown in Fig. 1, instead of the full sixteen motors and four generators [10]. The system components are shown in Table II and Fig. 1.

TABLE II
THE DESIGN PARAMETERS OF THE EA

Parameter	Quantity	Value
Generator	1	14.91 MW, 6 kV
Motor	4	1.86 MW
AC/DC Rectifier	1	14.91 MW
DC/AC Inverter	4	1.8 MW
SFCL	4	I_{rate} = 320 A, $I_{critical}$ =900 A
	1	I_{rate} = 1.28 kA, $I_{critical}$ =2.7 kA

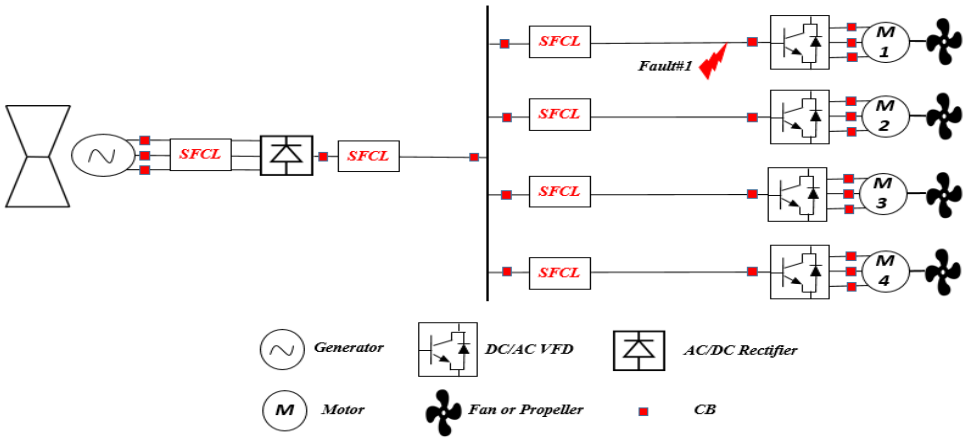

Fig. 1: One set of the EA with one generator, AC/DC rectifier, DC/AC inverter, four motors.

The ratings of the generator, motors, and converters are based on the data of the aircraft proposed by NASA [10]. The propulsion system is required to produce 22.5 MW for maximum thrust during take-off [15]. Because each motor can produce 1.86 MW thrust, at least 12 motors are required to work at the same time to ensure safe operation. The voltage DC-link is rated at 6 kVDC, as recommended by NASA [16]. In the proposed architecture, propulsion is provided by surface permanent magnet synchronous motors (SPMSM), which were chosen for their high power density and efficiency [17], the stator phase resistance is 24.21 mΩ. A non-salient, synchronous machine is chosen to model the characteristics of the generator with a stator resistance of 26.86 mΩ. The on-state resistance of the IGBTs used in the converter is estimated to be 1.5 mΩ. The fault current will be applied on the branch feeder as shown in Fig. 1. Different types of faults will be demonstrated: pole-to-pole, pole-to-ground with low grounding impedance.

3. Superconducting Fault Current Limiter (SFCL)

A SFCL is a self-mechanism electrical device which limits the fault current when a fault occurs, all within a few milliseconds, thus allowing the electrical network's protection system (switchgear, circuit breakers, etc.) to operate safely [18].

Because the EA has an on-board compact electrical network with high fault current levels, this level of fault current, if not properly managed, may exceed the maximum ratings of the protection systems, such as switchgears or circuit breakers, and consequently permanently damaging several devices such as generators, motors and cables via burnout. However, the use of the SFCL can reduce the fault current level to ensure safe operation for the protection system of the electrical network.

In general, SFCLs are classified into two main types: Resistive SFCL (R-SFCL) and Inductive (I-SFCL). Because the I-SFCL is heavier and more complex than the R-SFCL [19,20]and the weight is a crucial point in EA design, the focus of this paper will be on the R-SFCL type. The schematic circuit of a traditional R-SFCL is shown in Fig. 2.

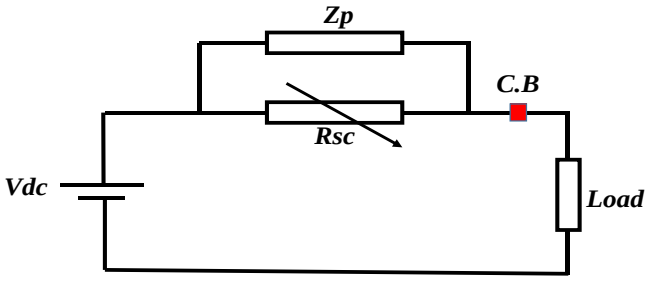

Fig. 2: Electric circuit of a resistive SFCL with parallel impedance

The two most common materials used to construct the SFCL are Yttrium Barium Copper Oxide (YBCO) and Bismuth Strontium Calcium Copper Oxide (BSCCO); both categorized as high temperature superconductors (HTS). In this study, YBCO is chosen to be the material of the R-SFCL for its better performance [20,21].

Two variables that control the behavior of the SFCL are the critical temperature and critical current density. The resistance of the R-SFCL can be calculated by the following equations:

$$J_c(T) = J_{co}\left(\frac{(T_c - T(t))^a}{(T_c - T_o)^a}\right) \qquad T_o < T < T_c \tag{1}$$

$$\rho_{HTS} = \frac{E_c}{J_c(T)}\left(\frac{J}{J_c(T)}\right)^{N-1} \qquad T < T_c\,, \quad J > J_C \tag{2}$$

$$\rho_{cu} = (0.0084T - 0.4603) \times 10^{-8} \qquad T > T_c \tag{3}$$

$$R_{sc} = \rho_{sc}\,\frac{l}{A} \tag{4}$$

$$T(t) = T_o + \frac{1}{C_p}\int_0^t Q_{sc}(t)dt \tag{5}$$

$$Q_{sc}(t) = P_{diss}(t) - P_{cooling}(t) \tag{6}$$

where J_{co} is the critical current density of the tape at the initial temperature. The initial temperature is the normal operation temperature, assumed here as the boiling temperature of liquid nitrogen (77 K). a is the density exponent and is equal to 1.5, which is applicable to YBCO material [22]. The critical temperature of YBCO T_c is equal to 92 K. When the current is less than the critical current of the YBCO material, the YBCO tape works in a superconductive state, meaning it has zero resistance, $\rho_{sc} = 0$. However, when the current exceeds the critical current value, the resistivity of the HTS layer increases sharply, according to Eq. 1. Ec = 1 μV/cm, which represents the electrical field. For the YBCO tapes, the N value ranges between 21 and 30. Eq. 2 is only valid when the temperature is less than the critical temperature and the current density is higher than the critical current density $J > J_C$. Under these two conditions the YBCO tape resistivity is equal to the resistivity of the superconducting layer, $\rho_{sc} = \rho_{HTS.}$ However, when the temperature exceeds the critical temperature, the resistivity of the HTS layer becomes higher than the resistivity of the copper stabilizer, thus most of the current goes through the copper layers and $\rho_{sc} = \rho_{cu}$. The resistivity of the copper layers depends on the temperature, as shown in Eq. 3. The resistance of the superconducting tape can be obtained from the resistivity of the HTS layer ρ_{HTS} from Eq. 2, and the resistivity of the copper stabilizer ρ_{cu} from Eq. 3, respectively. The HTS tape resistance is calculated using Eq. 4 where l is the length of the tape and A is the cross-sectional area of the tape. The temperature of the tape is calculated through Eq. 5 where Q_{sc} is the corresponding net power in the tape and C_p is the specific heat capacity of the material, which describes the amount of heat needed to increase the temperature of the material by one degree. In Eq. 6, $P_{diss}(t)$ represents the dissipated power in the superconducting tape and $P_{cooling}(t)$ is the cooling power representing the energy absorbed by the cooler. $P_{cooling}(t)$ reduces the temperature rise during a fault and brings the tape to a superconductive state after the fault.

TABLE III
THE DESIGN PARAMETERS OF SFCL

Parameter	Value
Critical Current (A)	300
Width (mm)	12
Total thickness (mm)	0.1
Copper stabilizer thickness (μm)	40
Length of YBCO tape (m)	233
Number of wires in parallel	3
Rated voltage (kV)	6
Resistance (Ω) @100 K	0.614
Resistance (Ω) @300 K	3.34

This paper focuses on the design of the four SFCLs on the branches shown in Fig. 1. The parameters of the SFCL are determined in Table III based on the initial fault analysis. The wire used in this paper is a 12 mm wide and 0.1 mm thick YBCO wire with a minimum critical current of 300 A (SCS12050) [23]. To build a 3.34 Ω @300 K YBCO tape with a copper stabilizer, three parallel 10 Ω @ 300 K tapes are used, each consisting of 233 m of superconducting tape. The critical current rating of this SFCL is 900 A.

4. Electric Aircraft Grounding System

All electrical systems must be grounded for several reasons, including enabling the detection of ground faults, as well as protecting human life and equipment, but the main goal is to redirect the vast amount of current during fault scenarios. In traditional electrical networks, the metallic part of equipment is connected to the earth. This is to provide an alternate high-voltage discharge path on the outside if the equipment's insulation fails for any reason as shown in Fig. 3(a). If the equipment is not earthed, these dangerous voltages can be transferred to anyone who touches it, resulting in an electric shock [24], [25]. However, connecting an aircraft to the earth is not possible at 30,000 feet, and thus the airframe (fuselage) is used for the grounding system instead.

The airframe can be made from different materials, including aluminum alloys as shown in Fig. 3(b). Because aluminum alloys are good conductors, the airframe can act as the traditional grounding (earth) which could be used as grounding, bonding, voltage reference and a current return path due to its high electrical conductivity, thereby reducing the number of wires on-board the aircraft by half [26].

As the power system architecture used in this paper is a DC power system based on the proposed N3-X architecture, the grounding system will be based on a positive pole, a negative pole as a return path, and the airframe as a ground, as shown in Fig. 3(c). The pole-to-pole fault is not affected by the different airframe or grounding technique because the return path of the fault is the negative pole. However, pole-to-ground faults are affected by changes in the airframe or the grounding technique.

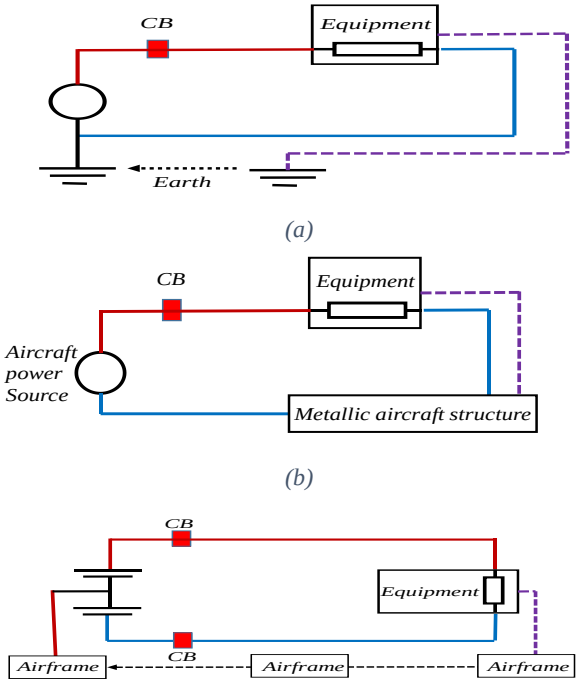

Fig. 3: Electric Grounding Systems: (a) Traditional, (b) Metallic Airframe, (c) DC-based EA

5. Simulation Results & Discussion

In order to investigate the fault behaviour in EA, the power system architecture of the EA shown in Fig. 1 is modelled in the MATLAB/Simulink system environment. The distance from the VSC to the DC bus is estimated to be 40 m and the distance from the DC bus to the motor's VFD is 5 m based on [10]. The resistance and inductance from the VSC to the fault position (assumed here to be at the end of the DC line as shown in Fig. 1) is 4.088 mΩ and 25.22 uH based on [27]. The DC-link capacitor is calculated to be 40 mF to ensure stable voltage on the DC-link. Two different types of faults are demonstrated in this section: a pole-to-pole fault and a pole-to-ground with low impedance grounding (0.1 Ω). A pole-to-pole fault is the most hazardous fault types due to the high voltage level between the positive and negative pole (+3 kV to -3 kV) and the low line impedance. On the other hand, a pole-to-ground fault occurs when either the positive or negative pole is connected directly to the ground. The most common type of short circuit is a pole-to-ground fault, yet it is not as critical as a pole-to-pole fault [28] ,[29]. For all results in this section, the circuit breakers do not trip, showcasing the performance of the SFCL device.

5.1 Case Study 1: Pole-to-Pole Fault

A pole-to-pole fault is applied at the location "Fault #1" on the feeder of the motor M1 shown in Fig. 1 for 100 milliseconds from t=2.0 s to t=2.1 s. Fig. 4(a) shows the voltage on the DC bus with and without SFCL, while the current of the feeder is shown in Fig. 4(b) with and without SFCL. Fig. 4(c) shows the AC voltage of the variable frequency drive (VFD) on the non-faulted branches, without SFCL. To show the effect of the fault on motors on the non-faulted branches, the motor speed of M4 from Fig. 1 is shown in Fig. 4(d) with and without SFCL.

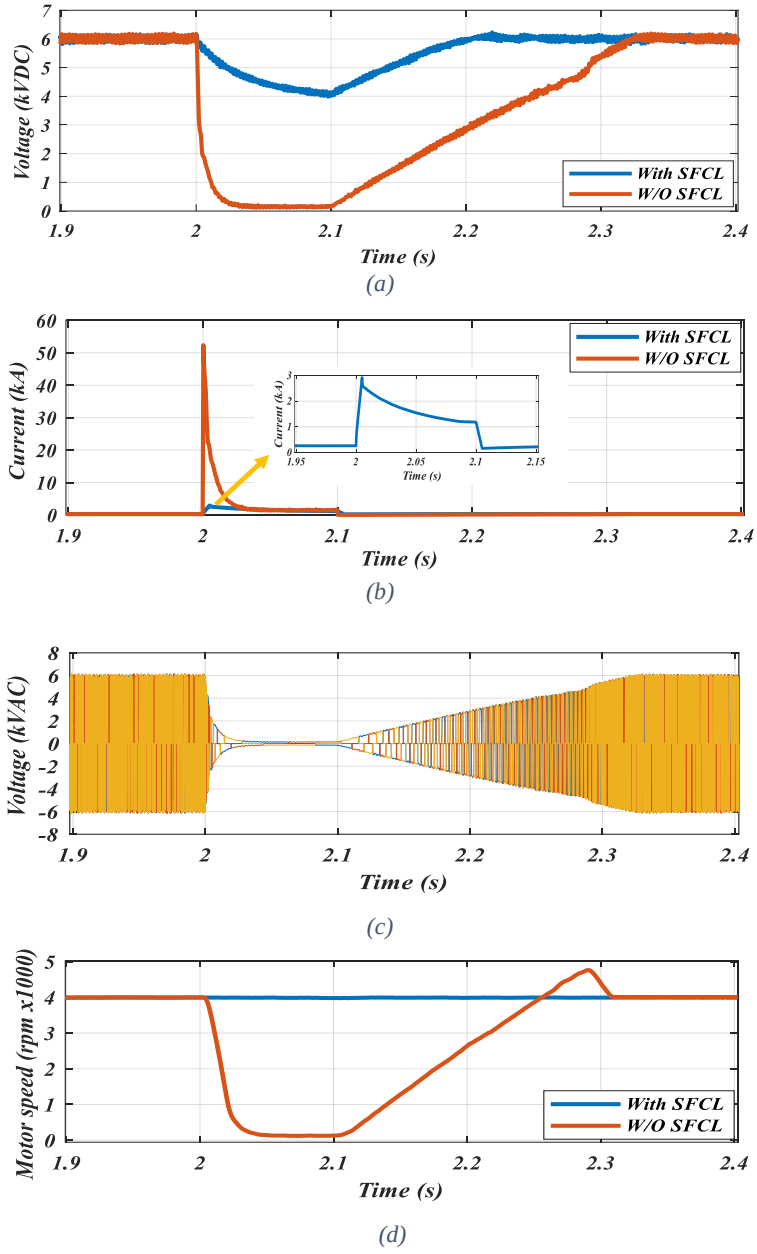

Fig. 4: Pole-to-pole fault current on the propulsion side at Fault#1 (a) Voltage at the DC bus with and without SFCL (b) Current at the motor branch with and without FCL (c) AC voltage on the non-faulted branches without SFCL (d) Motor speed M4 with and without SFCL.

The rated voltage of the DC bus is 6 kVDC. When the fault current occurred at t=2.0 s, the voltage of the DC bus dropped from 6 kVDC to almost zero without SFCL. With the SFCL however, the voltage only dropped to 4 kVDC for just few milliseconds. The rated current of each branch is 320 A. When the fault occurred, the current rose to almost 52 kA without the SFCL, whereas with the SFCL, the current was limited to 3 kA. The AC voltage of the VFD connected to motors on the non-faulted branches is shown in Fig. 4(c). When observing the speed of the motors on the non-faulted branches (specifically M4 here), the SFCL was able to maintain the desired speed, while the motor fed the fault then went into overdrive before eventually stabilising without the SFCL as shown in Fig. 4(d).

5.2 Case Study 2: Pole-to-Ground Fault with Low Impedance Grounding

A pole-to-ground fault is applied at "Fault #1" as shown in Fig. 1 with low impedance grounding (0.1 Ω) for 100 milliseconds from t=2 s to t=2.1 s. Fig. 5(a) shows the DC bus voltage with and without the SFCL, while the current of the faulted branch is shown in Fig. 5(b) with and without SFCL. Fig. 5(c) shows the AC voltage of the VFD on the non-faulted branches, without SFCL. The motor speed of M4 from Fig. 1 is shown in Fig. 5(d) with and without SFCL.

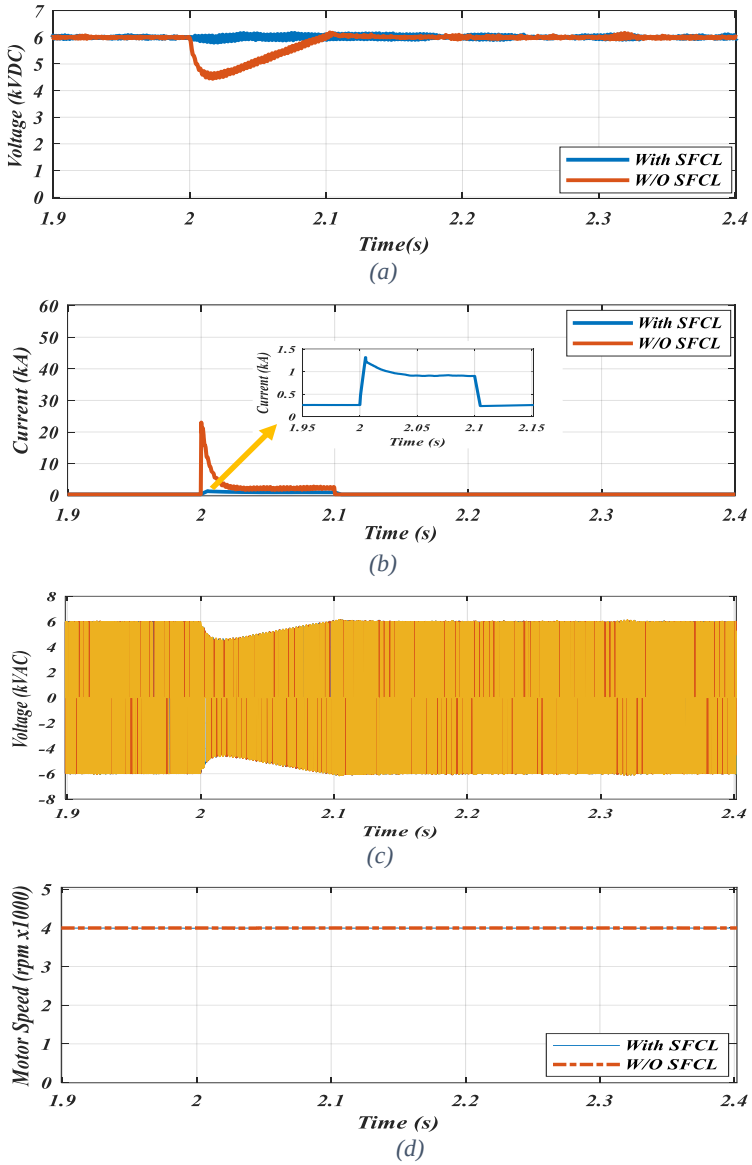

Fig. 5: Pole-to-ground fault current with low ground impedance (0.1 ohm) on the propulsion side at Fault#1 (a) Voltage at the DC bus with and without FCL (b) Current at the motor branch with and without SFCL (c) AC voltage on non-faulted branches without SFCL (d) Motor speed M4 with and without SFCL.

The voltage drop of the pole-to-ground fault was lower and shorter in time than the pole-to-pole fault for two reasons. Firstly, the voltage difference is half of that in the pole-to-pole fault (+3 kV to ground compared to +3 kV to -3 kV, respectively). Secondly, the DC voltage controller in the AC/DC rectifier-imposed overvoltage on the healthy pole to compensate for the voltage drop on the faulty pole, thus maintaining the overall voltage of the DC bus at the required level. When the fault occurred, the current rose to almost 22 kA without the SFCL, whereas with the SFCL, the current was limited to 1.4 kA. The AC voltage of the VFD is shown in Fig. 5(c). Because the voltage drop of the main bus was small and short in time, the speed of the motor M4 remained stable even without the SFCL.

Both the pole-to-pole and pole-to-ground faults are very hazardous for the system. In the pole-to-pole fault, the voltage difference is 6 kV compared to 3 kV in the pole-to-ground. The resulting drop of the main DC bus's voltage was high, dropping from 6 kV to almost zero, which affected the stability of the other motors on the non-faulted branches as shown in Fig. 4(d). Meanwhile, in the pole-to-ground fault, the voltage drop was small, and the AC/DC rectifier-imposed overvoltage on the healthy pole, thus reducing the voltage on the faulty pole and the resulting fault current. These factors combined with the short duration of the fault resulted in the pole-to-ground fault not affecting the stability of the non-faulted branches. Thus, the SFCL is important for both types of faults to reduce the fault current level and to support the protection system, with it being especially critical during the pole-to-pole fault.

6. Conclusion

This paper investigated and analyzed the behavior of a proposed power system architecture of EA based on NASA N3-X during different fault current scenarios. Different types of faults were applied at the feeder that feeds the EA motor: pole-to-pole, and pole-to-ground with low impedance grounding. In addition, the SFCL responses were demonstrated to show the effectiveness of the SFCL on the system in each scenario. Because the EA has a compact electrical network on-board operating at a high voltage level and a small impedance line, the current rose from 320 A to almost 52 kA during the pole-to-pole fault with the SFCL absent. The SFCL was able to limit the fault current to around 3 kA, which is only 5.7 % of the fault current without it. The fault current of the pole-to-ground fault with low impedance grounding reached almost 22 kA, which is lower than during the pole-to-pole fault. That was due to the lower voltage difference and the voltage controller which reduced the voltage on the faulty pole and increased the voltage on the healthy pole, thus reducing the fault current. The SFCL in that case was able to again limit the fault current to around 1.4 kA which is 6.36% of the fault current in this scenario. In either case, the presence of the SFCL was critical in avoiding the excessive increase in fault current which would lead to permanent damage to other parts of the system. Additionally, that means that the rating of the circuit breaker necessary to interrupt such a fault would be much lower and would thus be smaller, saving valuable space on the aircraft for other components, passengers, luggage, and so on.

7. Acknowledgments

This work was funded as part of the U.K. EPSRC, Developing Superconducting Fault Current Limiters (SFCLs) for Distributed Electric Propulsion Aircraft: EP/S000720/1.

References

[1] K. L. Suder, "Overview of the NASA Environmentally Responsible Aviation Project's Propulsion Technology Portfolio," *48th AIAA/ASME/SAE/ASEE Jt. Propuls. Conf. Exhib.*, no. August, pp. 1–23, 2012, doi: doi:10.2514/6.2012-4038.

[2] ACARE, "Strategic Research & Innovation Agenda," 2017. https://www.acare4europe.org/sites/acare4europe.org/files/attachment/acare-strategic-research-innovation-volume-1-v2.7-interactive-fin_0.pdf.

[3] H. Alafnan *et al.*, "Application of SMES-FCL in Electric Aircraft for Stability Improvement," *IEEE Trans. Appl. Supercond.*, vol. 29, no. 5, pp. 1–6, 2019, doi: 10.1109/TASC.2019.2905950.

[4] A. H. Epstein, "Aeropropulsion for Commercial Aviation in the Twenty-First Century and Research Directions Needed," *AIAA J.*, vol. 52, no. 5, pp. 901–911, 2014, doi: 10.2514/1.J052713.

[5] B. Sarlioglu and C. T. Morris, "More Electric Aircraft: Review, Challenges, and Opportunities for Commercial Transport Aircraft," *IEEE Trans. Transp. Electrif.*, vol. 1, no. 1, pp. 54–64, 2015, doi: 10.1109/TTE.2015.2426499.

[6] Airbus Group, "E-Fan: The New Way to Fly," *Brochure*, 2015, [Online]. Available: http://company.airbus.com/service/mediacenter/download/?uuid=48b1bd2c-a428-4c65-82e5-ed3e923bd142.

[7] R. Thomson, N. Sachdeva, M. Nazukin, and N. Martinez, "Aircraft Electrical Propulsion – The Next Chapter of Aviation?," *Think Act*, pp. 1–32, 2017, [Online]. Available: https://www.rolandberger.com/publications/publication_pdf/roland_berger_aircraft_electrical_propulsion.pdf.

[8] Airbus Group, "Airbus, Rolls-Royce, and Siemens team up for electric future Partnership launches E-Fan X hybrid-electric flight demonstrator." http://www.airbus.com/newsroom/press-

releases/en/2017/11/airbus--rolls-royce--and-siemens-team-up-for-electric-future-par.html.
[9] F. Berg, J. Palmer, P. Miller, M. Husband, and G. Dodds, "HTS electrical system for a distributed propulsion aircraft," *IEEE Trans. Appl. Supercond.*, vol. 25, no. 3, 2015, doi: 10.1109/TASC.2014.2384731.
[10] M. J. Armstrong *et al.*, *Architecture, Voltage, and Components for a Turboelectric Distributed Propulsion Electric Grid*, no. July. 2015.
[11] M. J. Armstrong, C. A. H. Ross, and M. J. Blackwelder, "Trade Studies for NASA N3-X Turboelectric Distributed Propulsion System Electrical Power System Architecture," 2012, doi: 10.4271/2012-01-2163.
[12] D. E. A. Mansour and D. M. Yehia, "Analysis of 3-phase superconducting fault current limiters in power systems with inhomogeneous quenching," *IEEE Trans. Appl. Supercond.*, vol. 23, no. 3, pp. 1–5, 2013, doi: 10.1109/TASC.2013.2240431.
[13] N. Y. Kwon *et al.*, "The effects of a stabilizer thickness of the YBCO coated conductor (CC) on the quench/recovery characteristics," *IEEE Trans. Appl. Supercond.*, vol. 20, no. 3, pp. 1246–1249, 2010, doi: 10.1109/TASC.2009.2039864.
[14] D. M. Yehia and D. E. A. Mansour, "Modeling and Analysis of Superconducting Fault Current Limiter for System Integration of Battery Banks," *IEEE Trans. Appl. Supercond.*, vol. 28, no. 4, 2018, doi: 10.1109/TASC.2018.2814398.
[15] M. J. Armstrong, C. A. H. Ross, M. J. Blackwelder, and K. Rajashekara, "Propulsion System Component Considerations for NASA N3-X Turboelectric Distributed Propulsion System," *SAE Int. J. Aerosp.*, vol. 5, no. 2, pp. 2012-01–2165, 2012, doi: 10.4271/2012-01-2165.
[16] K. H. Paul Gemin, Tom Kupiszewski, and Arthur Radun, Yan Pan, Rixin Lai, Di Zhang, Ruxi Wang, Xinhui Wu, Yan Jiang, Steve Galioto and and A. C. William Premerlani, Jim Bray, "Architecture, Voltage and Components for a Turboelectric Distributed Propulsion Electric Grid (AVC-TeDP)," vol. 1, no. July, pp. 1–107, 2015, [Online]. Available: https://ntrs.nasa.gov/search.jsp?R=20150014237.
[17] S. Li and Z. Liu, "Adaptive speed control for permanent-magnet synchronous motor system with variations of load inertia," *IEEE Trans. Ind. Electron.*, vol. 56, no. 8, pp. 3050–3059, 2009, doi: 10.1109/TIE.2009.2024655.
[18] X. Pei, A. C. Smith, and M. Barnes, *Superconducting fault current limiters for HVDC systems*, vol. 80. Elsevier B.V., 2015.
[19] S. Naderi, P. Davari, D. Zhou, M. Negnevitsky, and F. Blaabjerg, "A Review on Fault Current Limiting Devices to Enhance the Fault Ride-Through Capability of the Doubly-Fed Induction Generator Based Wind Turbine," *Appl. Sci.*, vol. 8, no. 11, p. 2059, 2018, doi: 10.3390/app8112059.
[20] W. T. B. De Sousa, R. Dias, F. A. Da Silva, A. Polasek, and R. De Andrade, "Comparison between the fault current limiting performance of Bi-2212 bifilar components and 2G YBCO coils," *IEEE Trans. Appl. Supercond.*, vol. 23, no. 3, pp. 2–6, 2013, doi: 10.1109/TASC.2013.2238275.
[21] M. M. Aly and E. A. Mohamed, "Comparison between resistive and inductive superconducting fault current limiters for fault current limiting," *Proc. - ICCES 2012 2012 Int. Conf. Comput. Eng. Syst.*, pp. 227–232, 2012, doi: 10.1109/ICCES.2012.6408518.
[22] F. Liang, W. Yuan, C. A. Baldan, M. Zhang, and J. S. Lamas, "Modeling and Experiment of the Current Limiting Performance of a Resistive Superconducting Fault Current Limiter in the Experimental System," *J. Supercond. Nov. Magn.*, vol. 28, no. 9, pp. 2669–2681, 2015, doi: 10.1007/s10948-015-3102-x.
[23] Super Power Inc., "SuperPower ® 2G HTS Wire Specifications," pp. 2–3, 2011.
[24] Fluke Corporation, "Earth Grounding," 2011.
[25] F. J. Angelini and D. D. Shipp, "Characteristics of different power systems neutral grounding techniques: fact and fiction," pp. 8/1-810, 2002, doi: 10.1109/texcon.1991.123141.
[26] M. Terorde, H. Wattar, and D. Schulz, "Phase balancing for aircraft electrical distribution systems," *IEEE Trans. Aerosp. Electron. Syst.*, vol. 51, no. 3, pp. 1781–1792, 2015, doi: 10.1109/TAES.2015.140031.
[27] Nexans, "6-36kV Medium Voltage Underground Power Cables," p. 48, 2009, [Online]. Available: http://www.nexans.co.uk/UK/files/Underground Power Cables Catalogue 03-2010.pdf.
[28] X. Li, Q. Song, W. Liu, H. Rao, S. Xu, and L. Li, "Protection of nonpermanent faults on DC overhead lines in MMC-based HVDC systems," *IEEE Trans. Power Deliv.*, vol. 28, no. 1, pp. 483–490, 2013, doi: 10.1109/TPWRD.2012.2226249.
[29] M. Monadi, M. A. Zamani, J. I. Candela, A. Luna, and P. Rodriguez, "Protection of AC and DC distribution systems Embedding distributed energy resources: A comparative review and analysis," *Renew. Sustain. Energy Rev.*, vol. 51, pp. 1578–1593, 2015, doi: 10.1016/j.rser.2015.07.013.